3D Particle Surface Reconstruction from Multi-view 2D Images with Structure from Motion and Shape from Shading (Jan. 2020)

Shuo Wang, Tonghai Wu, Kunpeng Wang, Zhongxiao Peng, Ngaiming Kwok, and Thompson Sarkodie-Gyan, *Member*, IEEE

***Abstract*—Since wear particles usually contain valuable information about lubricant and wear condition of lubricated components, wear debris analysis is widely used to monitor machine/component wear. Current literature reports about the importance and necessity of 3-dimensional (3D) surface characterization of wear particles as opposed to 2D characterization. It may be borne in mind that traditional 3D analysis has been a synonym only for local surface morphologies for stationary particles. This results in large errors when irregular particles are under observation. A new 3D imaging methodology is proposed to reconstruct multi-view 3D surfaces for a moving particle whereby the target particle is passed through a microchannel with rolling motion, and recorded via a digital microscope. The multiple moving particles are tracked based on Kalman filter to obtain different-view images. Sparse and dense reconstruction of the particle surfaces are enabled by these images using Structure from Motion (SfM) and Shape from Shading (SfS) methodologies, respectively. The method was verified using real particles and evaluated by the results of Laser Scanning Confocal Microscopy. The proposed method is able to reconstruct wear particles under various perspectives, and the errors from the characterization parameters of the Areal are less than 20 %.**

***Index Terms*—Wear debris analysis, 3D feature extraction, Structure from Motion, Shape from Shading.**

I. Introduction

VALUABLE information about a wear process, including the wear severity and wear mechanism, can be revealed through wear debris analysis (WDA). On account of this notion, WDA has been adopted over the years as the primary candidate for wear diagnosis [1], [2]. However, this technique may provide marginal results by virtue of its empirical dependence on the identification of wear particles. Based on increasing demands for an accurate, reliable and efficient analysis process, there is an increasing emergence in the WDA by shifting from 2D to 3D analysis with the objective of acquiring more comprehensive and accurate information of particle morphologies. As significant 3D information, the surfaces have record their generation mechanism with obvious features, such as scratches on the surface of severe sliding particles and pits on the surface of fatigue particles. Therefore, further development of new methods for extracting comprehensive features is important for wear particle identification, which is critical for wear mechanism assessment.

Conventional WDA is based on 2D images, e.g., using ferrography [3], and morphological features are extracted from plane images of some typical wear particles for wear diagnosis [4], [5]. Artificial intelligence algorithms have recently been introduced to facilitate such processes [6]. However, there have been frequent occurrences of misidentifications due to the absence of the topography information of the wear particles, especially when they have an irregular shape in 3D. As an example, laminar, adhesive, and severe sliding particles often exhibit similar boundary features in their 2D projection images but have different topographies when viewed in 3D. Another factor contributing to the misidentifications is the lack of quantitative description of distinctive surface features which are critical for similar particles. In fact, there arises the urgent requirement for the acquisition of more comprehensive features for the accurate identification of different types of wear particles.

The emergence of electron microscopy makes it possible to acquire and extract 3D features from wear particles. Stereo Scanning Electron Microscopy (SSEM) [7], Laser Scanning Confocal Microscopy (LSCM) [8] and Atomic Force Microscopy (AFM) [9] have been used for the investigation of wear particles in 3D. These technologies provide more morphological information than the conventional 2D approaches. However, since the particle is fixed on the spectrum, these instruments provide the surface topography from a fixed view. Typical features required for the identification of the type of

Manuscript received August 6, 2019; revised December 2, 2019; accepted January 13, 2020. This work was supported in part by the National Natural Science Foundation of China (No. 51975455 and No. 51675403), and in part by K. C. Wang Education Foundation. (*Corresponding author: Tonghai Wu*).

S. Wang, T. H. Wu and K. P. Wang are with the Key Laboratory of Education Ministry for Modern Design and Rotor-Bearing System, Xi'an Jiaotong University, Xi'an, Shaanxi 710049, China (e-mail: wstyxjtu@163.com; wt-h@163.com; moyuansuishang@163.com).

Z. P. Peng and N. Kwok are with the School of Mechanical and Manufacturing Engineering, University of New South Wales, Sydney, 2052, Australia (e-mail: z.peng@unsw.edu.au; nmkwok@unsw.edu.au).

T. Sarkodie-Gyan is with the Department of Electrical and Computer Engineering, University of Texas at El Paso, El Paso, USA (e-mail: tsarkodi@utep.edu).

wear particle may be omitted due to deposition randomness. Added to this is the fact that the complexities involved in the operation of these instruments, and coupled with their high costs, their application in industry has been greatly marginalized.

A video-based method has been reported for the acquisition of multi-view 2D images from moving particles [10]. The 3D model of wear particles is reconstructed, and the volume is estimated to evaluate wear severity in [10]. However, the established model for 3D image reconstruction may not accurately represent a particle because only the shapes of two-view images are used in the reconstruction. An improvement of this approach is later made through the extraction of 2D features from multi-view images for the statistical determination of 3D features [11]. Furthermore, the 3D model of the particles is constructed by using a silhouette-based method from full-view images [12]. Cutting, laminar and spherical particles are identified with the application of 3D features extracted from the 3D model. However, due to limitations in the image resolution and the reconstruction method in that work, 3D surface topographies of wear particles with similar boundary and surface features cannot be extracted reliably and utilized effectively for particle identification. Typical particles falling into this category are laminar, adhesive, and severe sliding particles, which often exhibit some similarity in 2D images acquired by ferrography.

A new 3D surface reconstruction methodology is hereby proposed through the integration of multi-view image acquisition and 3D reconstruction for moving wear particles. With a specifically designed oil channel, multi-view images of each rolling particle are acquired from the captured video by digital camera. A two-step algorithm is developed to reconstruct wear particle surfaces. In the first instance, sparse reconstruction is carried out based on SfM to accurately determine the spatial position of feature points on the wear particle surface. This is followed by a SfS-based dense strategy to enrich detailed features for sparse points. This two-step framework can ensure that wear particles are reconstructed with satisfactory accuracy.

The rest of this paper is organized as follows: Section II contains the description of the procedures involving the acquisition of multi-view particle images, the SfM-based sparse reconstruction, the SfS-based dense reconstruction, and the multi-view surfaces for wear particles. The verification of the proposed method is given in Section III, followed by discussions in Section IV. Main conclusions are presented in Section V.

II. Materials and Methods

A. Framework of the proposed method

A novel method for the surface reconstruction of wear particles using multi-view images is proposed in this work. With a similar design as the previous study [13], a moving wear particle acquisition system is established to capture the rolling particles through a digital camera via a microscope. In the system, micro-pump is selected as the driving force of oil to accurately control the flow rate from 1ml/h to 1000ml/h. The resolution of the digital camera is 1280 pixel $\times$ 960 pixel, and its physical size represented by each pixel is 0.75μm. A single-view light source, instead of ambient illumination, is used to illuminate wear particles to enhance the stereo information on the wear particle surfaces, and a high incidence angle is adopted for irradiating particle surfaces. The framework of this method is shown in Fig. 1 and the procedures involving three main steps are summarized as follows.

Step 1 Multi-view image acquisition: This first step is to acquire multi-view particle images with adequate surface morphological information. Videos of moving wear particles are captured with the designed system. Multi-view images are collected by applying a feature-based Kalman filter in tracking multiple particles found in the videos.

Step 2 Sparse reconstruction: This second step establishes a sparse characterization for the wear particle surfaces. The two images are selected from the multi-view image sequences of the wear particles (generally, the largest surface of a particle contains more surface characteristics). Feature points are handled by the Kanade-Lucas-Tomasi (KLT) operator and their spatial coordinates are calculated with SfM. To establish a relationship, spatial points are triangulated as shown in the box marked with "SP".

Step 3 Dense reconstruction: This third step provides a fine characterization for the wear particle surfaces. A dense strategy is constructed by adding points to triangulated sparse points obtained in Step 2. One of the images constructed in Step 2 is transformed and smoothened to obtain a luminance image. With this image, the relative heights of all points on the wear particle surface are reconstructed using the SfS method. The true height of the dense points is calculated based on the dense strategy and shown in the box marked with "RS".

Further details of the above 3 steps are presented in the sections below.

B. Multi-view image acquisition

In most cases, multiple particles simultaneously appear in the field of the observation with varying speeds. Meanwhile, the same particle is imaged with different boundary and/or surface features in images captured from different views. This causes some difficulties in the automatic collection of the multi-view image of the moving particles. To cope with these situations, a cooperative strategy is established based on the Kalman filtering. This consists of the following procedures: a) particle position estimation, b) feature matching, and c) tracking model updating.

1) Particle position estimation

For multi-target tracking, the estimation of possible location can reduce the search time. Because the flow velocity of the lubricant is constant, a constant velocity model can be adopted to predict particle position across frames. As a linear optimal estimation algorithm, Kalman filtering can transform the global search problem into local search for the sequential state of dynamic systems. Therefore, Kalman filtering is introduced

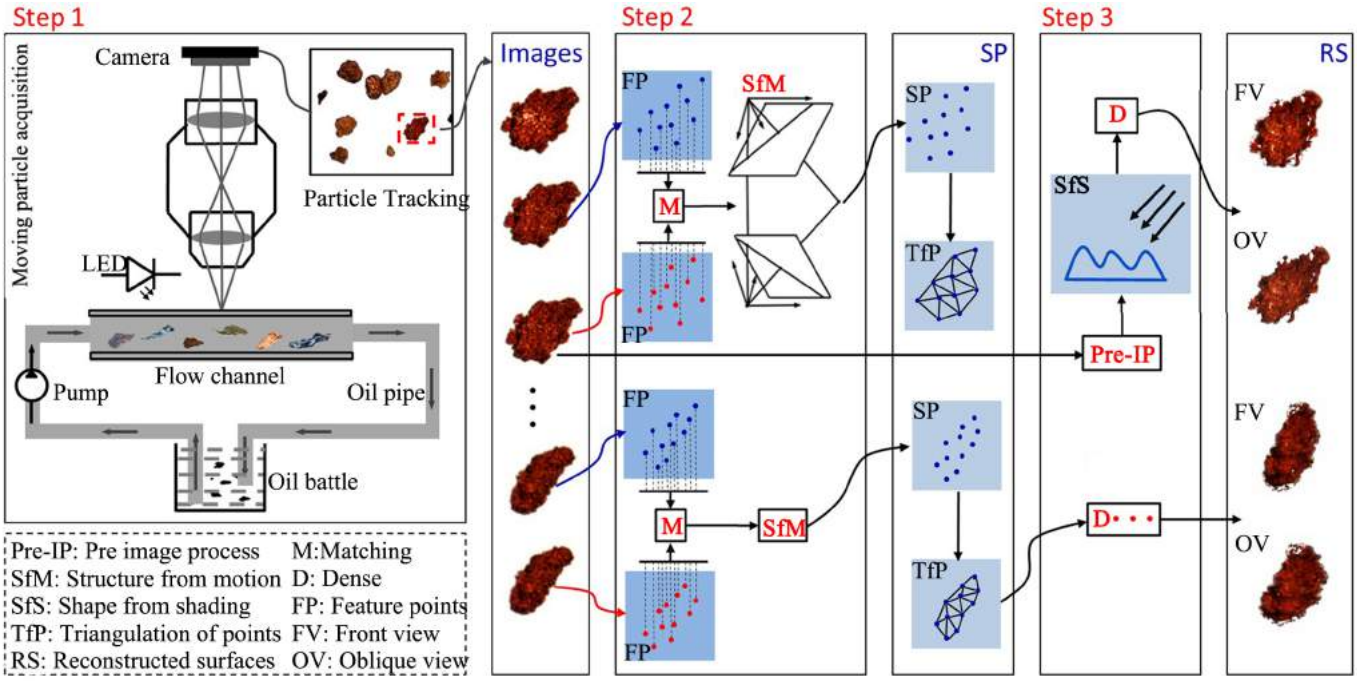

Fig. 1. The framework of the integrated system for moving particle acquisition and particle reconstruction in 3D.

to estimate the position of wear particles using their historical position information.

Accurate description of historical position information can facilitate particle tracking. During the movement of particles, the particle centroid and morphological characteristics continuously alter. A bounding rectangle composed of particle characteristics (including maximum length(L), minimum width (W), x coordinate of the center and y coordinate of the center), is projected to cover the whole wear particle, as shown in Fig. 2 (a). Meanwhile, these features change slowly as the particles rotate. Therefore, the historical position of the moving particle at the k^{th} frame is described with these particle features, as:

$$X_k = [L, v_L, W, v_W, x, v_x, y, v_y]^T \tag{1}$$

where v_L, v_W, v_x and v_y are the velocities of L, W, x and y over the k^{th} frame.

With the historical position description, the Kalman filter based estimation process is conducted with the prediction equation [14].

$$X_{k+1|k} = AX_k + W_k \tag{2}$$

where A is the state transition matrix which is determined by the moving features of the particle. W_k is correction term, its initial value is 0.

2) Feature matching

To cope with multiple particles existing in the predicted area, the target particle is identified with a feature matching process. Due to the low motion and high sampling rate (30fps), a reasonable assumption may be made that the appearance of the objective particle would not change dramatically. Therefore, the perimeter and area are chosen as the features to establish the matching criterion as:

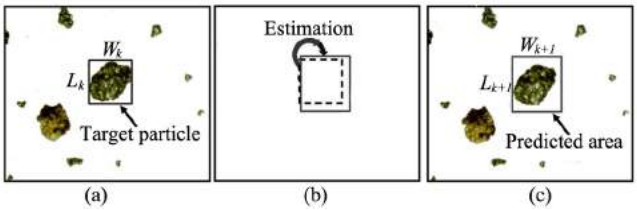

Fig. 2. Position estimation based on Kalman filtering: (a) tracked particle in the k^{th} frame, (b) position estimation, (c) predicted area in the $(k+1)^{th}$ frame.

$$\triangle_i = \gamma \frac{(A_k - A^i_{k+1})}{A_k} + (1-\gamma)\frac{C_k - C^i_{k+1}}{C_k} \tag{3}$$

where $\triangle_i$ is the degree of matching, A and C represent the perimeter and area of the target particle, respectively, i represents the i^{th} particle in the predicted area, k represents the k^{th} frame, γ is the weight of area and perimeter. As the wear particles rotate, both area and perimeter will change in time. Therefore, γ is defined as with an intermediate value (0.5).

$\triangle_i$ is adopted to characterize the degree of matching between the i^{th} particle in the search area and the target particle. Due to the high sampling frequency and slow rotation speed, wear particles will not change dramatically. With the statistical results of the change of moving particles in different sizes and speeds, 0.1 is determined as an effective threshold. When $\triangle_i$ is less than the threshold T (0.1), the two particles are considered as same one; i.e., the i^{th} particle is the tracked particle of the target particle in the next frame.

3) Tracking model updating

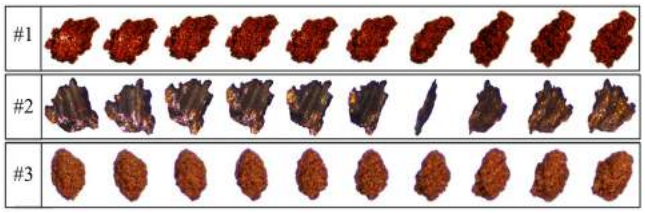

Fig. 3. Extracted multi-view images of three moving particles.

With the obtained target particle, the historical position of the moving particle at the $(k+1)^{th}$ frame can be updated as X_{k+1}. Considering the uncertainty in the movement, a more accurate estimation of W_k is carried out with Kalman filter for further predicting particle position in the next frame. By repeating particle position estimation, feature matching and tracking model updating, an automatic tracking is achieved for the moving wear particles. An example of extracted multi-view images of three moving wear particles is shown in Fig. 3. As can be observed, these wear particles show different morphological features on 2D images with changing captured views.

C. Sparse reconstruction

With weak surface texture information in the captured images, particle surface topography may not be directly reconstructed to a satisfactory level through the commonly used methods for 3D reconstruction. Therefore, a two-step algorithm is developed including a sparse and a dense reconstruction. The aim of the sparse reconstruction is to calculate the space coordinates of the key points which characterize the topography of the wear particle surfaces. A SfM-based reconstruction is adopted to calculate the 3D space coordinates of each key point. In order to obtain the maximum number of key points to characterize the surface, the feature points are extracted and matched from the two adjacent images. Furthermore, space position of feature points is calculated by analyzing the camera motion.

1) Feature point extraction and matching based on KLT

The surface topography information of an object exists in the form of feature points in the 2D image. Hence, 3D reconstruction can be carried out for wear particle surfaces by collecting a series of matched feature points from two sequential images [15], and the number of feature points directly determines the number of sparse reconstructions.

Weak surface textures lead to difficulties in the extraction of sufficient feature points to enable the characterization of the particle surfaces using conventional SIFT and HARRIS operators. Comparing the principles of the different feature point extraction methods, the KLT operator is selected to extract feature points from wear particle images. For the KLT operator, it is assumed that an image pixel is represented as $I(x,y)$, and a fixed window (W) can be established for the pixel in its adjacent area, which has a luminance value [16]. The corresponding feature extraction matrix G and feature equation $f(\lambda)$ are defined in Eqs. (4) and (5).

$$G = \begin{bmatrix} \sum_W I_x^2 & \sum_W I_x I_y \\ \sum_W I_x I_y & \sum_W I_y^2 \end{bmatrix} = \begin{bmatrix} a & b \\ c & d \end{bmatrix} \tag{4}$$

$$f(\lambda) = \lambda^2 - (a+b)\lambda + ac - b^2 \tag{5}$$

where I_x is the gradient in the x direction, I_y is the gradient in the y direction, and λ is the eigenvalues of the feature extraction matrix G. W is a fixed window in the pixel adjacent area. Considering feature extraction accuracy and computation time, 31 pixels $\times$ 31 pixels is an appropriate size.

According to Tomasi and Kanad in [17], Eq. (6) is chosen as the criterion for the feature point extraction. Should the value of the parameter a be larger than a pre-defined threshold λ_{HT}, this point is considered as a feature point. λ_{HT} is set to a small value (0.001) to improve the extraction accuracy of feature points. The extracted feature points are shown in Fig. 4. As it can be seen, extracted feature points are sufficient to cover the wear particle surface.

$$\begin{cases} f(\lambda_{HT}) > 0 \\ a > \lambda_{HT} \end{cases} \tag{6}$$

The feature points in the subsequent frames are matched with optimal estimation of the similarity between two feature points. According to the KLT algorithm, the solution of the matched feature points is equivalent to finding an optimal displacement d (d=($\triangle x$,$\triangle y$)) to minimize the sum of the squared intensity differences (SSD, denoted by ε), which can be calculated with Newton-Raphson iteration [18], [19].

$$\varepsilon = \int\int_W [J(X+d) - I(X)]^2 \omega(X) dX \tag{7}$$

$$\begin{aligned} d_{t+1} = d_t + \begin{bmatrix} g_x^2 & g_x g_y \\ g_x g_y & g_y^2 \end{bmatrix} \times \\ \left[\int\int_W [J(X) - I(X)] \begin{bmatrix} g_x \\ g_y \end{bmatrix} \right] d(X) \end{aligned} \tag{8}$$

where I and J represent two images, d_t represents the displacement of the feature window center, d_{t+1} represents the value calculated by the $(t+1)^{th}$ Newton iteration, g represents the first order coefficient of Eq. (7) carried out by Taylor.

The initial iteration value d_0 is set to 0. When the image points are iteratively matched to the termination condition: $|d_{x_{t+1}} - d_{x_t}|$ or $|d_{y_{t+1}} - d_{y_t}|$ is less than the set threshold 0.01, the displacement d is considered as an optimal value. Similarly, the matching is terminated when the number of iterations exceeds 30 (an empirical value).

2) Space position calculation of feature points

Establishing the corresponding relationship between 2D feature points and 3D surface points is a key step in reconstructing 3D surfaces from 2D images, and the relationship is determined by the geometric imaging model of the camera. Within the context of image processing as illustrated in [20], a point in space maps to pixels in image and this relationship can be expressed mathematically in Eq. (9).

$$sm' = K[R|t]M = \begin{bmatrix} f_u & 0 & u_0 \\ 0 & f_v & v_0 \\ 0 & 0 & 1 \end{bmatrix} [R|t]M \tag{9}$$

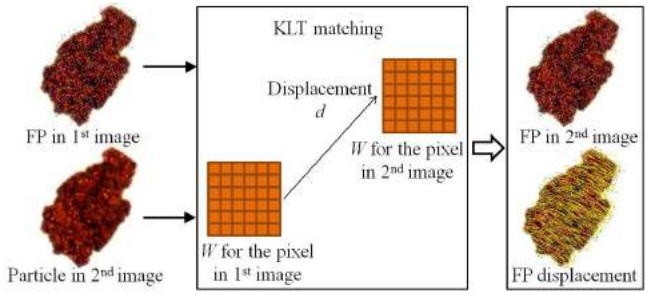

Fig. 4. Feature point (FP) matching between two adjacent images.

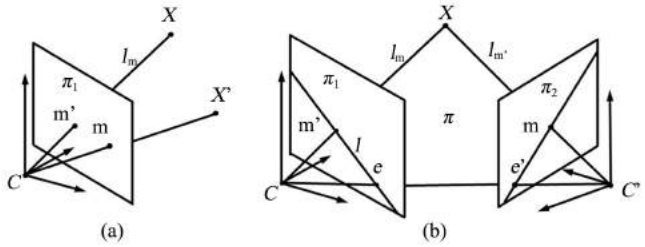

Fig. 5. Camera imaging model: (a) imaging model of moving wear particles; (b) transformed imaging model.

where s is the scale factor, m' is the 2D coordinates of the image, K is the camera intrinsic matrix, R is the rotation matrix, t is the translation matrix, M is the 3D coordinate in space, u_0 and v_0 are the coordinates of the pivot point (the point of the optical axis with the imaging plane), f_u and f_v are the focal lengths of the camera on the u-axis and v-axis, respectively.

Using Zhang's calibration method [21], the camera intrinsic matrix is estimated in our previous work presented in reference [22], and K is calculated as:

$$K = \begin{bmatrix} 34043.51 & 0 & 863.53 \\ 0 & 33376.80 & 430.49 \\ 0 & 0 & 1 \end{bmatrix} \tag{10}$$

The videos of the moving wear particles are collected with the same microscope at a fixed position, and the imaging model of the collection of the two-view images is shown in Fig. 5 (a). By changing the relative space position, it is assumed that the wear particles are stationary and the microscope-camera is rotated and shifted to the position C' to capture the second image. The transformed imaging model is shown in Fig. 5 (b).

Without loss of generality, the origin of the spatial coordinate system is located at the camera center of the first image. As a result, the translation vector t of the first image is $(0,0,0)^T$ and the rotation matrix R may be concluded as R=I. And, the projection matrix of the camera of the first image may be expressed as:

$$P_1 = K[I|0] = [K|0] \tag{11}$$

where I is a 3×3 unity matrix.

Compared with the spatial coordinate system established for the first image, the rotation matrix R and translation vector t (relative to the first image) for the second image

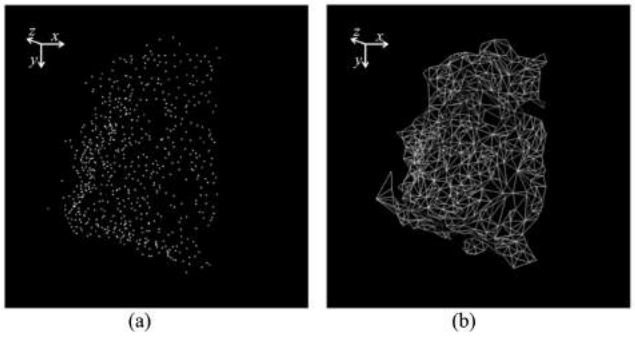

Fig. 6. Sparse reconstruction of wear particle surface: (a) spatial point clouds; (b) triangulation of point clouds.

can be calculated from matched feature point sets. According to Hartley in [23], feature point sets are pre-processed by normalization to enhance the stability of data. Eight feature point sets are randomly and uniformly selected to calculate the basic matrix and the intrinsic matrix. With the singular value decomposition of an intrinsic matrix [24], [25], the rotation matrix R and translation vector t are calculated for the second image. Using the same camera, the camera intrinsic parameter K remains unchanged, which was obtained by Zhang's calibration method. Thus, the projection matrix of the camera of the second image is expressed as:

$$P_2 = K[R|t] \tag{12}$$

With the obtained projection matrices of the two images and the imaging model in Eq. (9), a linear equation set can be established for each pair of the feature points, as:

$$\begin{cases} s_1 m_1' = P_1 X_w \\ s_2 m_2' = P_2 X_w \end{cases} \tag{13}$$

where X_w is the homogeneous coordinates of spatial 3D points $X_w = (X, Y, Z, 1)$, m_1' and m_2' represent the homogeneous coordinates of feature points $m_1' = (u_1, v_1, 1)$, and $m_2' = (u_2, v_2, 1)$ onto two images.

The set of equations in Eq. (13) contains 6 equations and 5 unknowns. Thus, the spatial coordinate of each matched point can be calculated using the least square method. Fig. 6 (a) is a spatial point cloud reconstructed from the adjacent two particle images in Fig. 4. In order to establish the relationship between the spatial points, point clouds are meshed by the Delaunay triangulation method [26] satisfying some criteria such as different side, maximum angle of normal vector, maximum/minimum inner angle, and the maximum number of used edges. The result is shown in Fig. 6 (b).

D. Dense reconstruction

As shown in Fig. 6, the wear particle reconstructed through the sparse reconstruction process exhibits its overall contour but lacks detailed surface textures. This is because the number of the feature points used for the 3D reconstruction is limited to represent the true surface of the wear particle. There arises the need to collect as many feature points as possible from the 2D images in order to characterize the wear particle with adequate surface topography information. Conventional

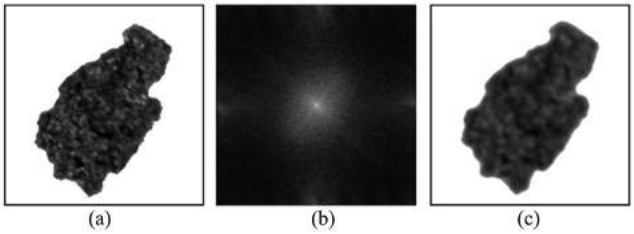

Fig. 7. Y-channel image preprocessing: (a) Y-channel image; (b) translated spectrum image; (c) image with Gaussian filter.

dense methods (such as PMVS [15]) fail to achieve dense reconstruction with limited sparse points. The SfS algorithm is able to reconstruct a relative 3D height for the visible pixels of a 2D image through the application of the shade change. With the relative height for the wear particle surfaces, dense reconstruction is carried out on sparse points. The main steps include: a) image preprocessing, b) surface reconstruction, and c) dense strategy.

1) Image preprocessing

The SfS method reconstructs a 3D surface based on the brightness change of images, whereas the color that existed on the wear particle surface may result in a poor reconstruction outcome. It is necessary to transform the color space to a luminance map instead of the original image for the SfS-based reconstruction. By comparing RGB, HSI and other color spaces, Luminance channel Y in YUV color space can reflect sudden changes of illumination intensity, and the transformation from RGB model to YUV model is linear which is able to avoid conversion overflow, as shown in Eq. (14). Therefore, the particle image in RGB color space is transformed into YUV color space to obtain a luminance map for the SfS-based reconstruction. The luminance channel Y is extracted from one of the two adjacent images used for sparse reconstruction, as shown in Fig. 7 (a).

$$\begin{bmatrix} Y \\ U \\ V \end{bmatrix} = \begin{bmatrix} 0.229 & 0.587 & 0.114 \\ -0.169 & -0.332 & 0.500 \\ 0.500 & -0.419 & -0.081 \end{bmatrix} \begin{bmatrix} R \\ G \\ B \end{bmatrix} \tag{14}$$

However, some noise (highlights) exists on the image in Fig. 7 (a), which will cause sudden changes in the reconstructed surface. With Discrete Fourier Transform (DFT), it can be observed that the noise is distributed in the high frequency band, as shown in Fig. 7 (b). Thus, noise components can be removed by filtering out the high frequency signals. Due to the property for preserving the gray distribution of an image, Gaussian filter is used to smoothen the wear particle images in the frequency domain. Highlights on Y-channel image have been eliminated as shown in Fig. 7 (c).

2) Surface reconstruction based on SfS

According to the Lambertian light reflection model [27], [28], the gray value of a point captured by the camera is concerned with the following four conditions (Fig. 8): the geometry of the object surface, the incident intensity and direction of the light source, the direction of the camera relative to the object, and the reflection characteristics of the object surface.

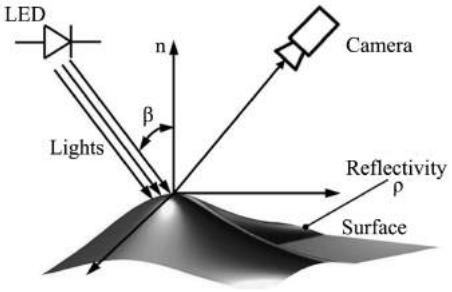

Fig. 8. SfS model for reconstructing the relative height of wear particle surface.

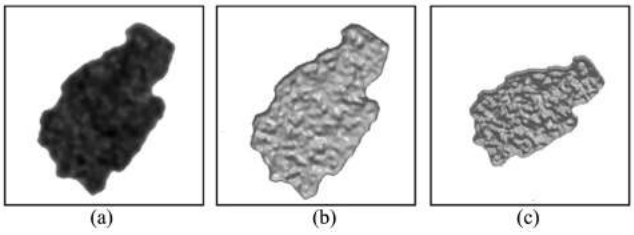

Fig. 9. SfS-based wear surface reconstruction: (a) luminance image; (b) front elevation of reconstructed surface; (c) oblique drawing of reconstructed surface.

With the reflection equation solution algorithm proposed by Tsai [29] and the Jacobi iteration [30], the height can be calculated for each pixel with Eq. (15).

$$Z^n(x,y) = Z^{n-1}(x,y) + [-f(Z^{n-1}(x,y))] \left[\frac{df(Z^{n-1}(x,y))}{dZ(x,y)}\right]^{-1} \tag{15}$$

where,

$$\frac{df(Z^{n-1}(x,y))}{dZ(x,y)} = -\frac{(p_s+q_s)}{(p^2+q^2+1)^{\frac{1}{2}}+(p_0^2+q_s^2+1)^{\frac{1}{2}}} + \frac{(p_s+q_s)}{(p^2+q^2+1)^{\frac{1}{2}}+(p_s^2+q_s^2+1)^{\frac{1}{2}}} \tag{16}$$

where $Z(x,y)$ is the height at pixel (x,y), (p,q) is the surface gradient of the object, (p_s,q_s) is the gradient of the incident direction of the light source.

Based on the experimental conditions, $Z^0(x,y)=0$, $p^0=0$ and $q^0=0$ are chosen as the initial variables. The incident light source is $p_s=0.908$ and $q_s=0.908$. The final surface height is obtained after completing the iterations, as shown in Fig. 9. It is found that although the SfS reconstructs the topographies of all visible areas, it only reflects the relative positions rather than accurate surface points. Therefore, the SfS-based reconstruction surface is adopted to dense sparse point reconstruction.

3) Dense strategy

The essence of dense reconstruction is to increase the number of points with certain rules and determine its spatial location. Based on the Delaunay triangulation method, geometric relations have been established for sparse points (see Fig. 6). Here, the midpoint of each side in every triangle

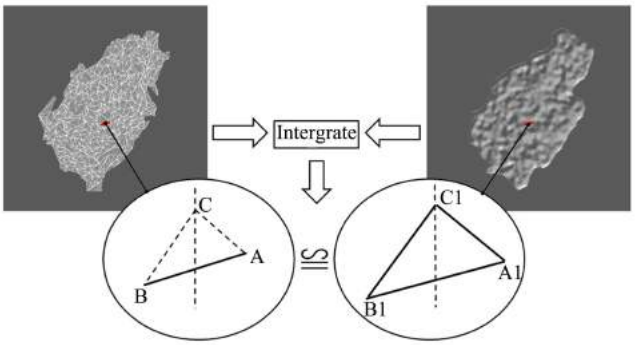

Fig. 10. SfS-based dense strategy for sparse points.

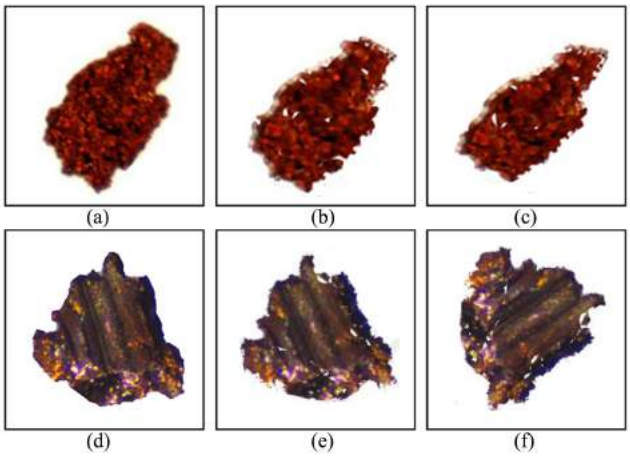

Fig. 11. Wear particle surface reconstructed based on SfM and SfS: (a) 2D image of wear particle #1 in Fig. 3; (b) front elevation of reconstructed surface for particle #1; (c) oblique drawing of reconstructed surface for particle #1; (d) 2D image of wear particle #2 in Fig. 3; (e) front elevation of reconstructed surface for particle #2; (f) oblique drawing of reconstructed surface for particle #2.

is selected as the dense point, as shown in Fig. 10, and its spatial position is calculated based on the Principle of Similar Triangles. Due to the small distance between two points A and B, it is assumed that the triangle composed of points A_1, B_1 and C_1 are similar to the triangle formed by points A, B and C. The relative position of points A_1, B_1 and C_1 are calculated by application of the SfS method, thus, the location of C can be uniquely determined.

The goal of the 3D reconstruction is to obtain the surface topographies of reconstructed objects, which should be close to the realistic object. Reconstructed 3D surfaces are more realistic and natural when surface textures are included. The original image is chosen as a texture map, and directly mapped onto the reconstructed wear particle surface. The surfaces of wear particles #1 and #2 in Fig. 3 are reconstructed, and different views of the final reconstruction results are illustrated in Fig. 11. Compared with the sparse points in Fig. 6, the grooves and parallel scratches on the particle surface can be clearly observed after the denseness of SfS.

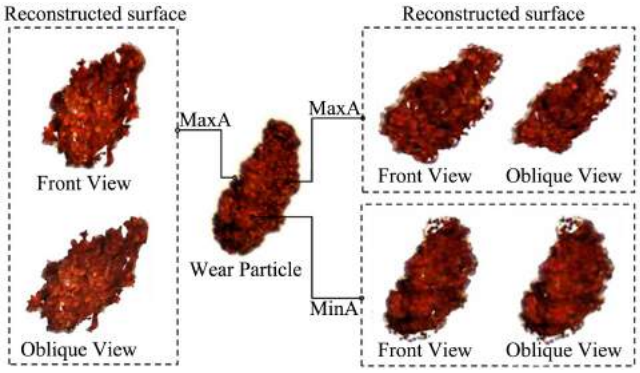

Fig. 12. Reconstructed surfaces from the wear particle in Fig. 3(a) under three views.

E. Multi-view surfaces of wear particles

Compared to existing 3D WDA methods, the most important advantage of the proposed method is that it provides multi-view surface topographies for a wear particle. From the multi-view images of the moving wear particle in Fig. 3(a), subsequent images of wear particles related to the maximum area (MaxA) and the minimum area (MinA) are selected and used to reconstruct the wear particle 3D surfaces. Reconstruction results are illustrated in Fig. 12. As demonstrated, the surface topography of the same wear particle is significantly different under different perspectives.

III. VERIFICATION

In this section, a set of comparative experiments is conducted to verify the performance of the proposed reconstruction method. A suitable process to evaluate the accuracy of 3D reconstruction is to compare a reconstructed surface with their respective references, when the 3D morphologies of the references can be obtained by existing instruments. As a 3D imaging instrument, LSCM has been successfully applied to particle surface analysis [8], thus it is used to verify the proposed method through the surface topography from a fixed view. First, the multi-view images of real particles are collected by the image acquisition system in Section II, and the wear particles are then collected and fixed to the glass slides. The 3D surfaces of the wear particles are firstly reconstructed with the LSCM. It further follows that the same view of wear particles are reconstructed by the proposed method. Three particle surfaces reconstructed from the two methods are shown in Fig. 13. As can be observed, there exists color deviations on the reconstructed surfaces with these two methods, which may be attributed to the different imaging conditions of the LSCM and moving particle acquisition system, such as lighting and exposure. But more importantly, the recovered surfaces by the proposed method exhibit a high similarity with the results from the LSCM, and the main characteristics, including surface grooves and bulges, have been reconstructed in the final particle surfaces.

In addition to the above evaluation of the effectiveness of the proposed reconstruction algorithm through visual inspection, quantitative analysis is carried out to further quantify the accuracy of the newly developed reconstruction approach.

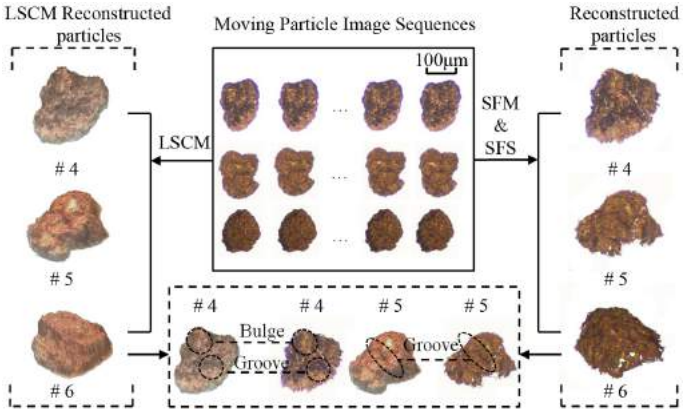

Fig. 13. Validation examples for the proposed method (Note: In order to highlight the surface details of particles, the particle images in Moving Particle Image Sequences are the part of real images that contain particles).

The 3D surface parameters of the micro-topography can comprehensively evaluate the complete surface rather than the contour; thus they are closer to reflect the real surface than 2D analysis. Furthermore, morphological features of wear particles are important for identifying the types of wear particles. Therefore, the accuracy of the proposed surface reconstruction is verified using surface topography parameters.

Areal parameter system is a 3D roughness evaluation method based on the middle surface of the topography. The parameters of the Areal characterization system are introduced in detail in ISO/TS CD 25178-2 [31]. Amongst these parameters, amplitude and functional parameters are reported to be closely related to distinctive features and are used to identify typical wear particles [32]. Three amplitude and two functional parameters are selected to characterize wear particle surfaces, including root-mean-square deviation (Sq), surface bearing index (Sbi), central liquid retention index (Sci), surface kurtosis (Sku) and surface skewness (Ssk).

The difference between the LSCM reconstructed surfaces and our reconstructed surfaces are recorded by extracting 3D surface parameters from particles in Fig. 13, and their values are reported in Table 2. It may be observed that most of the morphological information, especially for particles #4 and #6, are reconstructed with a good accuracy. As a result, although Sku and Sbi for particle #5 have a relative larger difference compared with the other parameters, the reconstruction accuracy is acceptable, indicating that reconstructed surfaces are very similar to the real ones and can be used to characterize typical wear particles.

TABLE I
PARAMETER COMPARISON BETWEEN LSCM RECONSTRUCTED SURFACES AND OUR RECONSTRUCTED SURFACES.

Particle	Parameter	LSCM	SfM&SfS	Errors
#4	Sq	49.03511	42.6475	13.03 %
	Sbi	0.5829	0.5746	1.42 %
	Sci	0.5829	0.5518	5.34 %
	Sku	0.0276	0.0310	12.32 %
	Ssk	1.3549	1.3208	2.52 %
#5	Sq	54.1600	57.6047	6.36 %
	Sbi	0.5659	0.6771	19.65 %
	Sci	0.5073	0.4956	2.31 %
	Sku	0.0275	0.0222	19.27 %
	Ssk	1.4914	1.2806	14.13 %
#6	Sq	61.6396	63.1083	0.24 %
	Sbi	0.5929	0.6785	14.44 %
	Sci	0.2664	0.2316	13.06 %
	Sku	0.0227	0.0194	14.54 %
	Ssk	1.3991	1.2242	12.50 %

IV. DISCUSSION

An integrating strategy for reconstructing multi-view 3D surface topographies of wear particles is presented based on SfM and SfS, involving three automated steps: multi-view image acquisition, sparse reconstruction, and dense reconstruction. A 3D surface is reconstructed by extracting feature points in two-adjacent frames. Using the same approach, multi-view 3D surfaces are reconstructed to characterize a wear particle through inputting two-adjacent frames from different perspectives. Comparing to conventional techniques for particle 3D surface reconstruction, this newly proposed reconstruction approach offers distinct advantages which are detailed below.

With respect to the video-based reconstruction system reported in previous works [11]–[13], the improvements of current works can be summarized as: a) A single-view light source is adopted in the acquisition system to enhance the details of particle surface; b) The current tracking method uses particle location estimation and feature matching instead of centroid tracking, which can reduce the matching error; c) The most important improvement is on the construction method of 3D feature. Previous work constructs 3D features of particles from 2D feature sequences, and successfully obtained the thickness of particles, but failed to describe the details of the particle surfaces, resulting in a low recognition of severe sliding, fatigue and other similar particles. The current work provides both surface features (such as surface kurtosis) and spatial features through using the integration approach of the SfM and SfS methods. When compared with conventional 3D particle imaging techniques [9], such as LSCM and SEM, the advantage of the proposed imaging method is that, the multi-view 3D surface topographies are acquired from different perspectives for a wear particle. This imaging method of a moving wear particle effectively avoids the loss of typical surfaces due to the deposition randomness of wear particles in the conventional 3D imaging techniques. Therefore, the newly proposed method is able to provide reliable and comprehensive 3D information of wear debris for wear analysis.

Apparently, three-view or more-view images introduced in the 3D reconstruction can increase the robustness of the reconstruction algorithm. However, there are still some problems to be solved in the reconstruction process. Due to the single-view

light source, the color reflected from particle surfaces may be different in multi-view images, which leads to the error of feature point matching. Simultaneously, the increase of multi-view images will need a new reconstruction method to deal with feature points in the different coordinates, which will further increase the complexity of the algorithm. Although it is important to improve the accuracy of surface reconstruction for the particle, a single particle can not reflect the wear type of the machine, which may be accidental or random. WDA is to analyze the machine wear state by all the particles produced during a running period. In addition, the results from the comparison have revealed that the surface reconstructed by the proposed method can reflect the main characteristics of the real particle surfaces, and it has achieved a high similarity with the reconstructed surface by LSCM. In view of the computational complexity and the reconstruction accuracy, the 3D reconstruction with two-view images is a suitable mean for wear particle surfaces.

Although the proposed method can reconstruct wear particle surfaces with satisfactory accuracy, the resolution is limited by the magnification/resolution of the digital camera used to acquire particle images. In addition, it will suffer performance degradation when occlusion occurs between two or more particles. This problem can be reduced by diluting the concentration of wear particles in the oil. The ultimate goal of this work is to improve the accuracy of wear particle identification. Therefore, future work will be carried out in the identification of wear particles based on multi-view 3D surfaces. With new 3D characterization and numerous intelligent identification algorithms [32], artificial intelligence-based wear particle identification may be implemented to further improve the efficiency and accuracy of WDA.

V. Conclusion

A new system for reconstructing multi-view 3D surfaces of wear particles from two-adjacent frames under different perspectives is presented. The main features are that: 1) the designed image acquisition system is able to collect multi-view 2D images of moving wear particles with appropriate stereoscopic information; 2) based on the KLT, feature points are extracted and matched from two subsequent images, and their space positions are calculated with the SfM to characterize the key topography points of wear particle surfaces; and 3) through integrating the relative height calculated using the SfS method, space points are increased to form dense wear particle surfaces with fine surface texture features. Using LSCM to evaluate the performance, it has been demonstrated that the surfaces reconstructed by the proposed method have a high similarity to the real surfaces. Compared with the existing 3D WDA approaches, this method offers a comprehensive characterization for individual particle by providing multi-view 3D surfaces for reliable and accurate wear particle identification.

References

[1] C. Haiden, T. Wopelka, M. Jech, F. Keplinger, and M. J. Vellekoop, "A microfluidic chip and dark-field imaging system for size measurement of metal wear particles in oil," *IEEE Sensors Journal*, vol. 16, no. 5, pp. 1182–1189, 2015.

[2] P. Feng, W. Liyong, and C. Tao, "Finite element simulation of onâline wear debris monitoring sensor based on jmag," in *2017 13th IEEE International Conference on Electronic Measurement & Instruments (ICEMI)*, pp. 196–200. IEEE, 2017.

[3] T. Wu, Y. Peng, H. Wu, X. Zhang, and J. Wang, "Full-life dynamic identification of wear state based on on-line wear debris image features," *Mechanical Systems and Signal Processing*, vol. 42, no. 1-2, pp. 404–414, 2014.

[4] S. Ebersbach, Z. Peng, and N. Kessissoglou, "The investigation of the condition and faults of a spur gearbox using vibration and wear debris analysis techniques," *Wear*, vol. 260, no. 1-2, pp. 16–24, 2006.

[5] Y. Zhang, J. Mao, and Y.-B. Xie, "Engine wear monitoring with olvf," *Tribology Transactions*, vol. 54, no. 2, pp. 201–207, 2011.

[6] W. Cao, W. Chen, G. Dong, J. Wu, and Y. Xie, "Wear condition monitoring and working pattern recognition of piston rings and cylinder liners using on-line visual ferrograph," *Tribology Transactions*, vol. 57, no. 4, pp. 690–699, 2014.

[7] G. Stachowiak and P. Podsiadlo, "Towards the development of an automated wear particle classification system," *Tribology International*, vol. 39, no. 12, pp. 1615–1623, 2006.

[8] Y. Tian, J. Wang, Z. Peng, and X. Jiang, "A new approach to numerical characterisation of wear particle surfaces in three-dimensions for wear study," *Wear*, vol. 282, pp. 59–68, 2012.

[9] J. Wu and Z. Peng, "Investigation of the geometries and surface topographies of uhmwpe wear particles," *Tribology International*, vol. 66, pp. 208–218, 2013.

[10] R. M. Dan, "Multi-view and three-dimensional (3d) images in wear debris analysis (wda)," Ph.D. dissertation, The University of Manchester (United Kingdom), 2013.

[11] T. Wu, Y. Peng, S. Wang, F. Chen, N. Kwok, and Z. Peng, "Morphological feature extraction based on multiview images for wear debris analysis in on-line fluid monitoring," *Tribology Transactions*, vol. 60, no. 3, pp. 408–418, 2017.

[12] H. Wu, N. M. Kwok, S. Liu, T. Wu, and Z. Peng, "A prototype of on-line extraction and three-dimensional characterisation of wear particle features from video sequence," *Wear*, vol. 368, pp. 314–325, 2016.

[13] Y. Peng, T. Wu, S. Wang, Y. Du, N. Kwok, and Z. Peng, "A microfluidic device for three-dimensional wear debris imaging in online condition monitoring," *Proceedings of the Institution of Mechanical Engineers, Part J: Journal of Engineering Tribology*, vol. 231, no. 8, pp. 965–974, 2017.

[14] S. Chen, "Kalman filter for robot vision: a survey," *IEEE Transactions on industrial electronics*, vol. 59, no. 11, pp. 4409–4420, 2011.

[15] Y. Furukawa and J. Ponce, "Accurate, dense, and robust multiview stereopsis," *IEEE transactions on pattern analysis and machine intelligence*, vol. 32, no. 8, pp. 1362–1376, 2009.

[16] W. Jang, S. Oh, and G. Kim, "A hardware implementation of pyramidal klt feature tracker for driving assistance systems," in *2009 12th International IEEE Conference on Intelligent Transportation Systems*, pp. 1–6. IEEE, 2009.

[17] C. Tomasi and T. Kanade, "Shape and motion from image streams under orthography: a factorization method," *International Journal of Computer Vision*, vol. 9, no. 2, pp. 137–154, 1992.

[18] B. D. Lucas, T. Kanade *et al.*, "An iterative image registration technique with an application to stereo vision," 1981.

[19] S. N. Sinha, J.-M. Frahm, M. Pollefeys, and Y. Genc, "Feature tracking and matching in video using programmable graphics hardware," *Machine Vision and Applications*, vol. 22, no. 1, pp. 207–217, 2011.

[20] R. Hartley and A. Zisserman, *Multiple view geometry in computer vision*. Cambridge university press, 2003.

[21] Z. Zhang *et al.*, "Flexible camera calibration by viewing a plane from unknown orientations." in *Iccv*, vol. 99, pp. 666–673, 1999.

[22] S. Wang, T. Wu, L. Yang, N. Kwok, and T. Sarkodie-Gyan, "Three-dimensional reconstruction of wear particle surface based on photometric stereo," *Measurement*, vol. 133, pp. 350–360, 2019.

[23] R. I. Hartley, "In defence of the 8-point algorithm," in *Proceedings of IEEE international conference on computer vision*, pp. 1064–1070. IEEE, 1995.

[24] J. J. Koenderink and A. J. Van Doorn, "Affine structure from motion," *JOSA A*, vol. 8, no. 2, pp. 377–385, 1991.

[25] L. De Lathauwer, B. De Moor, and J. Vandewalle, "A multilinear singular value decomposition," *SIAM journal on Matrix Analysis and Applications*, vol. 21, no. 4, pp. 1253–1278, 2000.

[26] T. Su, W. Wang, Z. Lv, W. Wu, and X. Li, "Rapid delaunay triangulation for randomly distributed point cloud data using adaptive hilbert curve," *Computers & Graphics*, vol. 54, pp. 65–74, 2016.

[27] B. K. Horn, "Height and gradient from shading," *International journal of computer vision*, vol. 5, no. 1, pp. 37–75, 1990.
[28] R. Zhang, P.-S. Tsai, J. E. Cryer, and M. Shah, "Shape-from-shading: a survey," *IEEE transactions on pattern analysis and machine intelligence*, vol. 21, no. 8, pp. 690–706, 1999.
[29] T. Ping-Sing and M. Shah, "Shape from shading using linear approximation," *Image and Vision computing*, vol. 12, no. 8, pp. 487–498, 1994.
[30] E. Rouy and A. Tourin, "A viscosity solutions approach to shape-from-shading," *SIAM Journal on Numerical Analysis*, vol. 29, no. 3, pp. 867–884, 1992.
[31] I. C. 25178-2, "Geometrical product specification (gps)–surface texture: areal–part 2. terms, definitions and surface texture parameters," 2012.
[32] Z. Peng and M. Wang, "Three dimensional surface characterization of human cartilages at a micron and nanometre scale," *Wear*, vol. 301, no. 1-2, pp. 210–217, 2013.

Shuo Wang received the Bachelor's degree in Mechanical Design Manufacture and Automation from Taiyuan University of Technology, Taiyuan, China, in 2014. He is currently working toward the Ph.D. degree in Mechanical Engineering from Xi'an Jiaotong University, Xi'an, China.

His research interests include machine condition monitoring, wear debris analysis and micro 3D surface analysis.

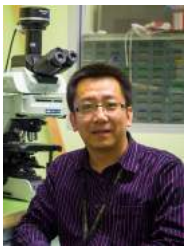

Tonghai Wu received the Ph.D. degree in Mechanical Engineering from Xi'an Jiaotong University, Xi'an, China, in 2006.

He is currently a Professor with the School of Mechanical Engineering, Xi'an Jiaotong University. From 2013 to 2014, he was a Visiting Scholar with University of New South Wales, Australia. His current research interests include machinery diagnosis and prognosis, machine vision on wear particle and surface analysis.

Kunpeng Wang received the Bachelor's degree in Mechanical Design Manufacture and Automation from Taiyuan University of Technology, Taiyuan, China, 2018. He is currently working toward the M.S. degree in Mechanical Engineering from Xi'an Jiaotong University, Xi'an, China.

His research interests include on-line visual ferrograph design and wear debris analysis.

Zhongxiao Peng received the Ph.D. degree in Mechanical Engineering from the University of Western Australia, Australia, in 2000.

She is currently a Professor in the School of Mechanical and Manufacturing Engineering, University of New South Wales. Her current research interests include wear analysis of mechanical and bio-engineering systems, 3D image analysis of worn surfaces and wear debris, vibration and vibration control, and artificial intelligence for mechanical system analysis.

Ngaiming Kwok received the Ph.D. degree at the ARC Center for Autonomous Systems, University of Technology Sydney, Australia, in 2007.

He is currently a Lecturer with the School of Mechanical and Manufacturing Engineering, University of New South Wales. His research interests include image processing, intelligent computation, and automatic control.

Thompson Sarkodie-Gyan received the Dr.-Ing. degree in Measurement and Control from Technical University, Berlin, Germany, in 1985.

He is currently an Associate Professor with the Department of Electrical and Computer Engineering, the University of Texas at El Paso. His current research interests include biomedical engineering, mechatronics systems engineering, robotics and automation, electrical measurements of non-electrical quantities, machine vision and pattern recognition, applications of soft computing, and sensors.